ARTICLE NO. 78-744R

Powering Prediction for Surface Effect Ships Based on Model Results

Robert A. Wilson,* Steven M. Wells,† and Charles E. Heber*
David W. Taylor Naval Ship Research and Development Center, Bethesda, Md.

A method employing the laws of dynamic similarity to scale experimental model data is presented for predicting the powering performance of large surface effect ships. The data are reduced to individual components, including cushion wavemaking drag, sidewall and appendage frictional and form drags, aerodynamic drag, and seal drag. These components are appropriately scaled by either Froude or Reynolds scaling laws. Water channel and model dimension effects on wavemaking drag are discussed and a technique for calculating sidewall wetted area is presented. An experimentally derived algorithm characterizing seal-induced and frictional drag is explained. Drag predictions are compared with experimental trials data.

Introduction

THE drag prediction technique presently used for scaling the model drag of a surface effect ship (SES) is different from that developed by Froude, in that both the frictional and wavemaking drag terms can be accurately determined. The basic drag components are broken down into two classes: 1) those which are due to lift provided by the pressure region which dimensionally (or Froude) scale, and 2) those which are due to friction and must account for skin-friction coefficient changes with Reynolds number between the model and the prototype. The first theories,[1] which were developed to describe the resistance characteristics of the SES, broke the components into the wavemaking drag due to the pressure region and the frictional drag of the sidewalls. Seal drag estimates were based on early British expressions derived for hovercraft. SES technology has been advanced significantly since these early estimations were made. The various drag components have been studied extensively, largely through model experiments, and are now understood in much greater depth.

The resistance of an SES is usually estimated either from a theoretical approach (which has usually been correlated with or supplemented by experimental data), or one whereby experimentally derived model data are used extensively. The theoretical approach is used in parametric or sizing studies where one examines the effect of weight, length-to-beam ratio, or other parameters of a generalized design. These parametric prediction programs, however, may not be adequate to estimate the impact of the sometimes subtle physical differences between specific designs such as sidewall deadrise angle or chine effects, airflow rate effects, or the inherent differences between planing or bag and finger seals. These design-related differences can only be evaluated adequately through the use of model experiments and the analysis of the data. This paper summarizes a technique used by the Navy to calculate the resistance of a large prototype SES based on model test data.

The insight into understanding these components has involved many breakthroughs over the last decade. The ability to measure the hydrodynamic forces on the seals in calm water as well as in seas has been a major advancement. The analysis of information contained in numerous model photographs, such as the seal and sidewall wetting shown in the photograph of the SES-100A-1 model in Fig. 1, has also been significant. Testing techniques and analysis procedures such as these have played a major role in the development of the SES.

Component Drag Discussion

The total drag D_T in the scaling program is broken down into components. The model aerodynamic drag component D_A is determined from specific model experiments. This value of D_A is later replaced by more appropriate wind-tunnel results. The wavemaking drag D_W of the pressure region of the cushion is calculated theoretically. The frictional drag component D_F is determined through an accurate definition of the sidewall and appendage-wetted areas. The component nominally referred to as the residual drag D_R is comprised primarily of the seal frictional and induced drag and the sidewall and appendage form drags.

Figure 2 presents a breakdown of these components as drag-to-weight ratios for the SES-100B as a function of Froude number (based on cushion length) in a state 1 sea. This figure shows the residual (seal) drag dominating at subhump

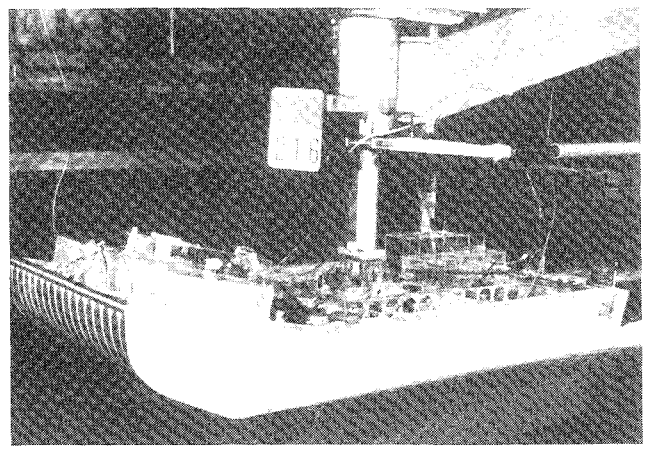

Fig. 1 SES model during powering experiments.

Received April 12, 1978; presented as Paper 78-744 at the AIAA/SNAME Advanced Marine Vehicles Conference, San Diego, Calif., April 17-19, 1978; revision received June 7, 1979.

Index category: Marine Hydrodynamics, Vessel and Control Surface.

*Aerospace Engineer, Aviation and Surface Effects Dept.

†Aerospace Engineer, Aviation and Surface Effects Dept. Member AIAA.

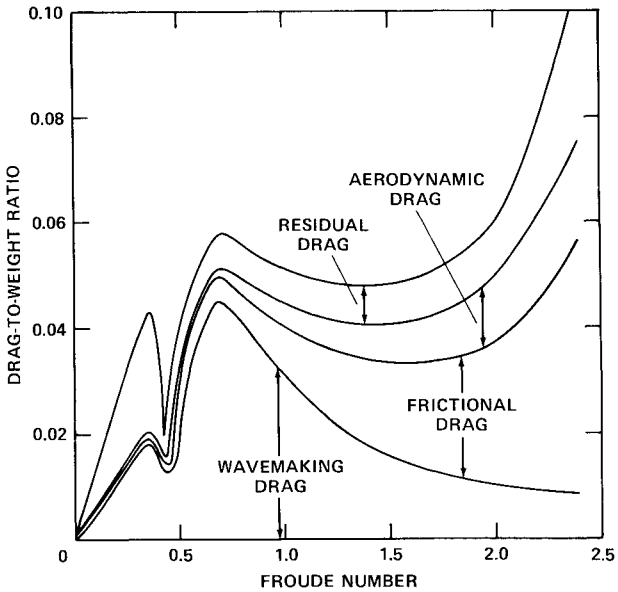

Fig. 2 Drag component breakdown for the SES-100B in state 1 sea.

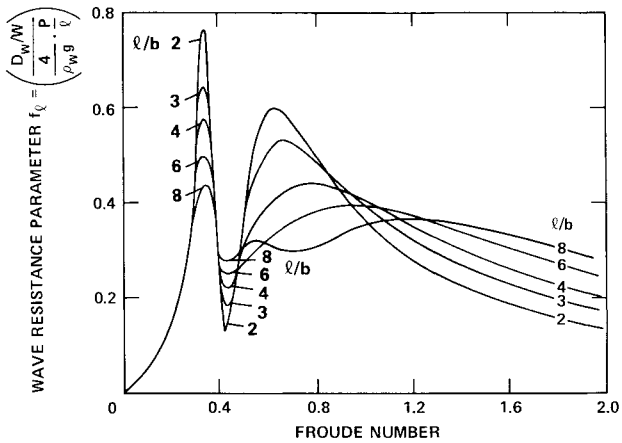

Fig. 3 Newman and Poole's wave resistance parameter.

speeds, wavemaking drag dominating at or near the hump speed, and frictional drag dominating at higher speeds. This component breakdown is typical for most designs, but can be influenced by design variations such as the seals or the spray rails.

The drag components are broken into drag-to-weight ratio D/W values. The total drag is then viewed as follows:

$$\frac{D_T}{W} = \frac{D_W}{W} + \frac{D_F}{W} + \frac{D_A}{W} + \frac{D_R}{W}$$

The following discussions in this paper deal with an understanding of these components and how they are scaled.

When working in model scale, one must understand dimensional scaling. Table 1 shows how the dimensions, forces, airflow relations, and speeds of the model scale to prototype size according to Froude scaling.

Wavemaking Drag

A vehicle moving through the water on a cushion of air generates waves due to the action of the pressure region on the water. This pressure region acts back on the vehicle to produce lift plus a wave drag component. Figure 3 presents plots of the wave resistance parameter f_ℓ as a function of Froude number for a family of length-to-beam ratio pressure regions, as determined from Newman and Poole's theory.[2] Note that the cushion pressure and length are key parameters

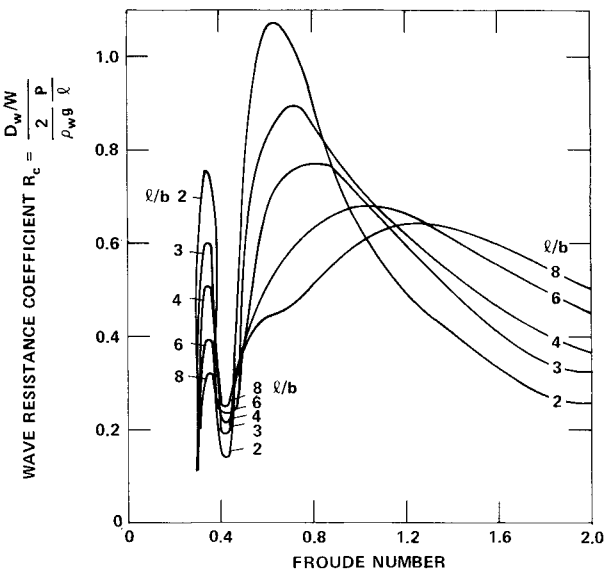

Fig. 4 Doctors' wave resistance coefficient.

in calculating the wavemaking drag once the wavemaking resistance parameter is known. The adequacy of this wavemaking drag calculation has been demonstrated for the air cushion vehicle. Experimental investigations into the wavemaking drag of a hovercraft were made in England by Hogben,[3,4] and have been shown to agree with Newman and Poole's theoretical predictions in Ref. 5. These experiments were conducted in such a manner that only the cushion acted on the water surface; no physical part of the model touched the water surface. Since the SES has rigid sidewalls and seals immersed in the water generating waves which interfere with the wave patterns generated by the pressurized field, the adequacy of the calculations again is questioned.

Model experiments were conducted to verify the use of Newman and Poole's predictions as well as to compare the experimental results with the wave resistance predictions of Doctors.[6] Doctors' predictions have pressure falloff parameters affecting the pressure region on the four sides. By varying these pressure falloff parameters, the shape of the wave resistance characteristics with Froude number vary, predominantly in the subhump region. The results of the experiments[7] showed that Doctors' predictions with pressure falloff parameter values of $\alpha = 5.0$ and $\beta = \infty$ matched the subhump data. Thus, Doctors' wave resistance coefficient (Fig. 4) is used for calculating the wavemaking resistance for an SES.

Because the cushion pressure is the key parameter in calculating the wavemaking drag and the wavemaking drag dominates in the hump region, the easiest way to verify wavemaking drag predictions is to vary the weight (and pressure) of the model and to compare the measured drag changes with predictions. This was done for the length-to-beam ratio 2.67 model and the results are shown in Fig. 5. This level of agreement demonstrates that the theory is adequate to predict this component for SES drag scaling. The spikes in the total resistance curve at the secondary hump

Table 1 Froude scaling relationships[a]

Length	$-\lambda$	Speed	$-\lambda^{1/2}$
Area	$-\lambda^2$	Pressure	$-\lambda$
Volume	$-\lambda^3$	Airflow rate	$-\lambda^{2.5}$
Force	$-\lambda^3$	Moments	$-\lambda^4$

[a] $\lambda = (\text{equivalent cushion length})_P/(\text{equivalent cushion length})_M$ and the subscripts P and M denote prototype and model, respectively.

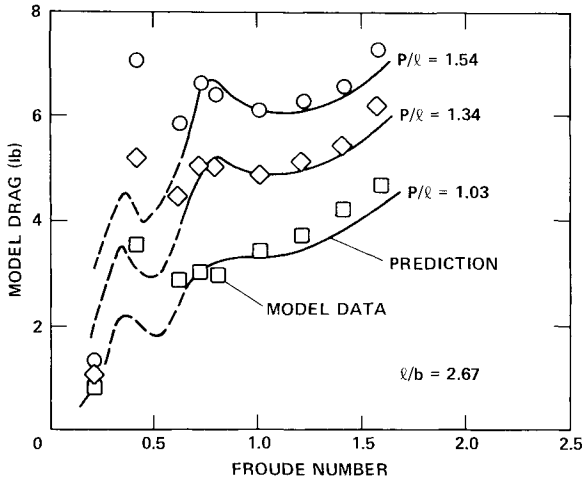

Fig. 5 Comparison of measured and predicted drag variations with pressure-to-length ratio.

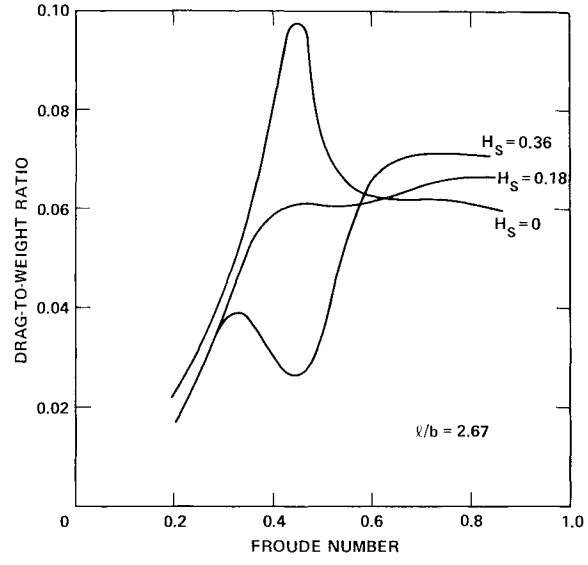

Fig. 6 Seal height effects on hump traverse.

(Froude number $\simeq 0.4$) are predominantly seal-induced and can be lowered by raising the seals above the keel while traversing the secondary hump as shown by the model result in Fig. 6. When the seals are raised from their normal position $H_S = 0$, where the trailing edge of the seal is at the keel, to a value of $H_S = 0.36$, where the seal has been raised 36% of the cushion height above the keel, the subhump drag has been reduced by more than a factor of 3. When the seal is raised 18% ($H_S = 0.18$), the subhump and hump drag values are nearly the same. Note, however, in Fig. 6 that the lowest drag at the primary hump (Froude number $\simeq 0.7$) is with the seals located at the keel ($H_S = 0$).

The following equation presents the wavemaking drag-to-weight ratio calculation for both the model and the prototype which are the same.

$$\left(\frac{D_W}{W}\right)_M = R_c\left(\frac{P}{\ell}\right)_M\left(\frac{2}{\rho_W g}\right) = R_c\left(\frac{0.9W}{b\ell^2}\right)_M\left(\frac{2}{\rho_W g}\right) = \left(\frac{D_W}{W}\right)_P$$

The value of the wave resistance coefficient R_c is determined from Fig. 4. The values of the beam b and length ℓ of the cushion are determined from the model or prototype drawings and $0.9W/b\ell$ replaces the pressure term. The preceding expression assumes that the water density of the model and the full-scale ships are the same. The water density

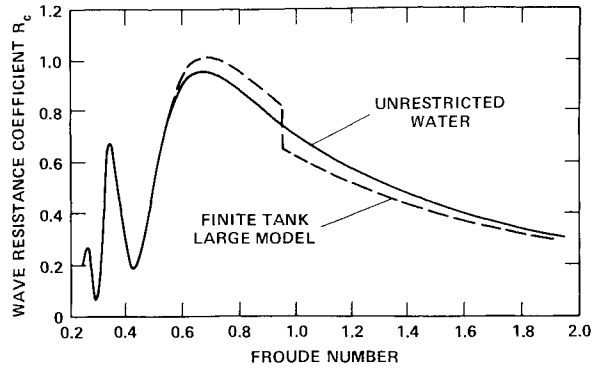

Fig. 7 Towing tank effects on wave resistance coefficient.

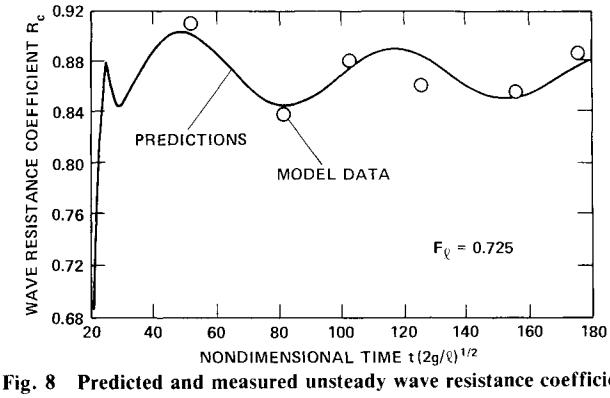

Fig. 8 Predicted and measured unsteady wave resistance coefficient at near-hump speed.

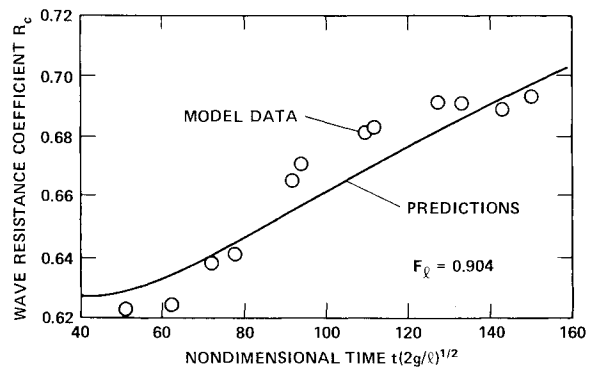

Fig. 9 Predicted and measured unsteady wave resistance coefficient at a marginally subcritical speed.

must be properly accounted for both in determining the model weight and the model and prototype wavemaking drag values.

The size of the model and the dimensions of the towing tank must be properly scrutinized when interpreting model data. The wave resistance curves in Figs. 3 and 4 are for the pressure region passing over an infinitely deep and wide body of water. The restricted towing basin does not always represent such a body of water. Figure 7 shows Doctors' predicted steady-state wave resistance coefficient for a large model operating in a towing tank; the infinitely wide and deep case is shown for reference. The discontinuity for the finite tank case occurs at the tank critical Froude number. The results of this figure show that substantial corrections in the wavemaking resistance may need to be made while testing in the restricted waters of the towing basin.

Doctors' unsteady wave resistance predictions have been verified by specific experiments at the David W. Taylor Naval Ship Research and Development Center. The results shown in Figs. 8-11 show the dependence of the wave resistance

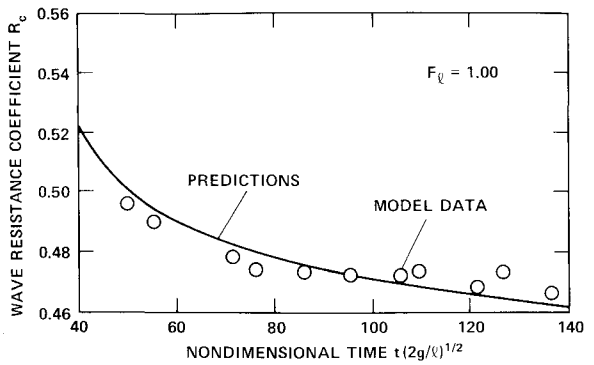

Fig. 10 Predicted and measured unsteady wave resistance coefficient at a marginally supercritical speed.

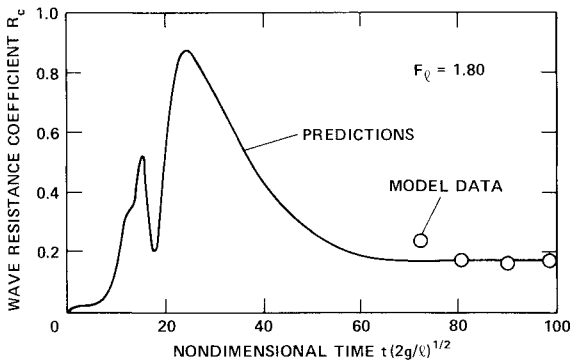

Fig. 11 Predicted and measured unsteady wave resistance coefficient at a high speed.

coefficient with nondimensional time in the restricted channel. Figure 8 compares the predictions with experimental data at a near-hump speed, while Figs. 9 and 10 show similar data at marginally subcritical ($F_\ell = 0.904$) and supercritical ($F_\ell = 1.00$) speeds. High-speed experiments ($F_\ell = 1.80$) show no variation with nondimensional time as shown in Fig. 11.

The wavemaking resistance component calculated from Fig. 4 is then corrected using the appropriate steady or unsteady values of R_c for the specific model and towing facility. Since this is a time-dependent problem, the acceleration rate of the carriage and point in time when data are taken in the towing tank must also be considered.

Frictional Drag

The frictional drag component D_F is computed using the relationship

$$D_F = C_f(\rho_W/2)V^2A$$

The two important considerations here are the values of the selected skin-friction coefficient C_f and the wetted area A used in the calculation. The wetted areas scale as λ^2 as previously shown, and C_f varies with Reynolds number. The following discussion describes the technique used to determine the wetted area and the proper skin friction coefficients.

Previous techniques for computing the wetted areas on the sidewalls have assumed that model heave and trim angles, as indicated from towing tank tests, produce an accurate representation of the actual sidewall wetting. Photographs and movies from model tests, however, indicate that at posthump speeds, wetted areas determined from the heave and trim data are consistently smaller than the actual wetted areas observed. Using the photographs from many model tests, an empirically derived relationship between wetted area, trim angle, and Froude number has been determined. The height of the chine or spray rail has been shown to have the

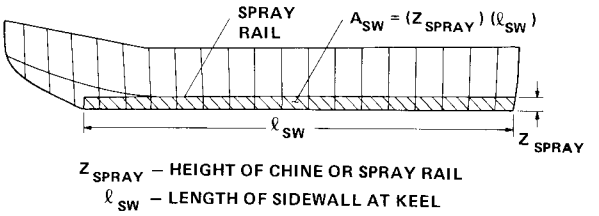

Fig. 12 Sidewall area below the chine A_{SW}.

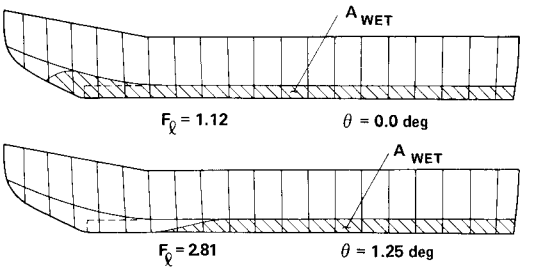

Fig. 13 Typical sidewall wetting.

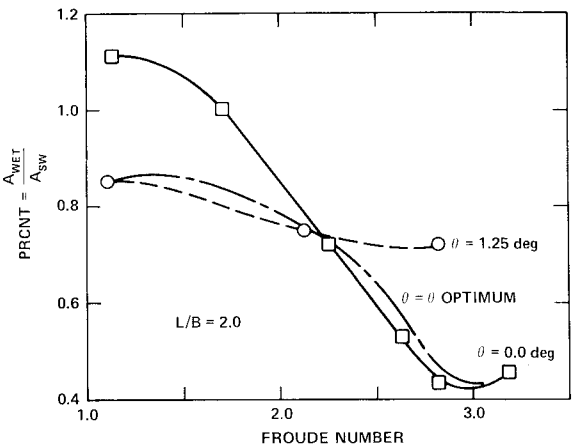

Fig. 14 Percent wetted area for low ℓ/b SES.

greatest effect on wetted area. Therefore, the projected sidewall area below the chine A_{SW} was used as a basis of comparison for determining sidewall wetting. The sidewall area A_{SW} is illustrated in Fig. 12 and is defined as the length of the sidewall at the keel times the average height of the spray rail or chine above the keel. The actual projected wetted area measured from test photographs A_{WET} was then expressed as a percentage of the sidewall area below the chine:

$$\text{Percent} = \frac{A_{WET}}{A_{SW}}$$

Typical sidewall wetting for an $\ell/b = 2.0$ SES at Froude numbers of 1.12 and 2.81 is illustrated in Fig. 13. The cases presented in Fig. 13 are for nonoptimum trims.

The ratio of the actual sidewall wetted area to the area below the chine A_{WET}/A_{SW} is plotted in Fig. 14 as a function of Froude number for various trim angles. Curves of percent wetted area for various fixed trim angles of this typical case are shown, as well as an estimation of the percent wetting at optimum trim which varies with speed. The curves will vary with length-to-beam ratio; those in Fig. 14 were determined for a model with a length-to-beam ratio of 2.0.

The technique of determining the sidewall wetted area becomes a matter of interpolating a value of percent wetted area for the given ℓ/b and trim angle. The projected wetted area A_{WET} is then calculated by multiplying the sidewall area

below the chine A_{SW} by the percent wetting

$$A_{WET} = \text{percent}\,(A_{SW})$$

Assuming a constant deadrise angle ϕ, the actual wetted area of the sidewall is determined by dividing the projected area by $\sin\phi$. The wetted area of any flat portions of the keel and the wetting on the cushion side of the sidewall are then added.

The inside wetting of the sidewalls at posthump speeds has been observed from photographs to be zero when the seals are set at the keel. If the seals are set above the keel, the inside wetting is calculated using the area between the keel and a straight line connecting the lower tips of the bow and stern seals. This straight-line approximation does not apply to subhump speeds, but because the frictional drag at these low speeds is small, the straight-line approximation is still applicable.

The preceding discussion applies to the calculation of sidewall wetting in calm water. In rough water, additional area must be added to account for the wetting from waves. This additional area is equal to the corrected average wave height $\bar{H}/2.5$ times the length of the sidewall and is added to the inside wetting. The outside of the sidewall is wetted to the spray rail or chine in calm water (see Fig. 13); therefore, operation in waves generally does not increase the outside wetted area over that observed in calm water.

To complete the calculation of full-scale friction drag, the model and ship skin-friction coefficients must be determined. The approach taken in the aircraft industry is used for the SES where surface roughness is evaluated (as opposed to that usually used by the ships community where the Schoenherr line is used with a ΔC_f added). The coefficient of friction is a function of Reynolds number and the equivalent sand roughness k_s of the sidewalls. Reynolds number is based on the sidewall length at the keel ℓ_{SW} which is approximately the wetted length. The sand roughness is an equivalent measure of surface irregularities on the outer skin. Most model sidewalls have smooth painted surfaces and have shown (through the use of a profilometer) that their roughness is nominally 1 mil.

A roughness of nominally 1 mil is also considered to be close to the roughness anticipated for a large vessel. This value, however, produces a value of C_f close to that determined from analysis of standard ship-scaling techniques and substantiated with some full-scale data. Hoerner[8] notes that the American Towing Tank Conference suggests that, due to ship roughness, a ΔC_f value of 0.0004 be added to the Schoenherr line C_{f_0}. In the Reynolds number range in question for large SES vehicles, this happens to yield an effective roughness of approximately 1 mil. This value of C_f was obtained from studies of displacement ships in the 15-20 knot range. An interesting observation by Hoerner is that the ratio of C_f of the ship (including roughness effects) to C_{f_0}, the value determined from the Schoenherr curve, increases as the speed capability increases. This fact seems reasonable when observing the C_f vs Reynolds number curves from Schlichting.[9] Schlichting shows that the slope of the smooth Schoenherr curve is always negative, whereas curves of constant ℓ/k_s values (characteristic length/roughness factor) become quite flat, and in some Reynolds number ranges, the slope is slightly positive. The comments made by Hoerner regarding this phenomenon were deduced from ship trials and seem to correlate well with the above-discussed C_f vs Reynolds number trend.

The value used for C_f can be determined from the following expressions for a wide range of vehicle sizes, roughness, and speeds. The first expression is the Prandtl-Schlichting derivation for the resistance of a smooth plate at zero incidence.

$$C_f = 0.455\,(\log_{10} R_n)^{-2.58}$$

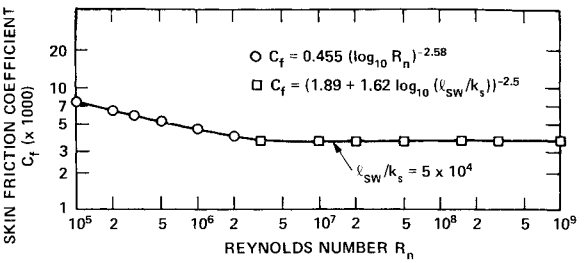

Fig. 15 Numerical computation of skin-friction coefficient.

This equation corresponds to boundary-layer flows that are turbulent and vary only as a function of Reynolds number. The second equation is derived for sand-roughened plates and corresponds to a fully turbulent boundary layer.

$$C_f = [\,1.89 + 1.62\log_{10}(\ell/k_s)\,]^{-2.5}$$

Both of these expressions are used, dependent on the Reynolds number and roughness. Figure 15 presents the skin-friction coefficient variation with Reynolds number for a roughness factor of 5×10^4 which is a typical value for a model. For low Reynolds numbers, such as are found on model appendages, sand separation strips should be used to assure turbulent flow. Model experiments of the sidewalls tested with and without sand separation strips show that the sidewalls are always in turbulent flow.

This discussion described how the skin-friction coefficients and wetted areas for both the model and the prototype are determined. Thus, the relationships between model and prototype frictional drag-to-weight ratios is as follows:

$$(D_F/W)_P = (D_F/W)_M\,(C_{f_P}/C_{f_M})$$

Some typical 1 mil skin-friction coefficient values are shown in Table 2. Appendage frictional drag is calculated in a manner similar to the sidewall frictional drag. Wetted areas can be determined from drawings.

Aerodynamic Drag

Hydrodynamic models poorly represent the aerodynamics of the prototype design. As shown in Fig. 1, the models normally do not have weather decks or superstructures. The local aerodynamic flows present near the model in the towing tank are similar neither in magnitude nor in direction to those expected in the open water due to boundary-layer differences and channel and carriage flow disturbances. Reynolds number effects also must be considered. Because of these differences, the aerodynamic forces on the hydrodynamic model are measured as tares using special test techniques. This model tare value for drag is subtracted from the measured model drag leaving only the hydrodynamic drag components. During the course of scaling the individual drag components, wind-tunnel data for the appropriate configuration is substituted.

The equation used to calculate the aerodynamic drag D_A of the prototype is:

$$D_A = C_{D_a}\,(\rho_a/2)\,V^2 A_f$$

Table 2 1 mil skin-friction coefficient values

Size	C_f
1/30-scale 3KSES model	0.0033
1/20-scale 3KSES model	0.0030
100-ton testcraft	0.0024
3KSES prototype	0.00195

where C_{D_a} is the aerodynamic drag coefficient. The reference area A_f is determined as the product of the overall beam and the height from the water to the weather deck. The aerodynamic drag coefficient can vary from 0.3 for a clean hull with no superstructure to 1.1 for a square design with a "dirty" superstructure. If no aerodynamic drag coefficient is available, a value of $C_{D_a} = 0.5$ can be used for a reasonably designed craft.

Residual Drag

Residual drag D_R is the drag component remaining after subtracting the previously described components from the total model drag. In terms of drag-to-weight ratio, this becomes

$$\frac{D_R}{W} = \frac{D_T}{W} - \frac{D_F}{W} - \frac{D_W}{W} - \frac{D_A}{W}$$

The residual drag component is predominantly comprised of the momentum drag, sidewall and appendage form drag, and seal drag. The momentum and form drags are relatively small quantities; the seal drag term represents the major portion of the residual drag term.

The momentum drag occurs when the constant mass flow entering from the fans into the cushion is brought from a particular velocity to zero velocity relative to the craft. In addition, a cushion thrust is produced by the flow exiting under the stern seal. The magnitudes of these two forces are equal within experimental accuracy, and because the forces are opposing, the sum of the momentum drag and cushion thrust are assumed to be zero.

The sidewall and appendage form and pressure drag terms D_P are small but not negligible. Both can be computed using simple techniques. For both, the form drag is equal to the submerged cross-sectional area multiplied by the average head of water displaced. This computational technique works very well for the sidewalls. The appendages may require a correctional term to account for appendage shaping. This, however, can be done on a case-to-case basis. Both the sidewall and appendage form drags D_P are Froude scaled.

The remainder and the larger portion of the residual drag term, then, is predominantly seal drag. Scaling seal drag involves the breakdown of seal drag into seal-frictional and seal-induced drag components. These components, once determined, then must be scaled independently.

The determination of the magnitude of the seal forces was accomplished by testing an SES model, segmented and instrumented to isolate the loads acting on the bow and stern seal. Figures 16 and 17 show a setup photograph and a schematic of the model as tested. As shown, the model consisted of three segments. One was the bow seal module, which contained the bow seal, a small portion of the wetdeck, and a short portion of the sidewall. The second module was the centerbody and stern seal module which comprised the bulk of the wetdeck and to which the stern seal was attached. The third module was the sidewall-support module which held the bulk of the sidewall. The three modules were attached to each other by means of two balances, yielding measured forces as shown in the schematic. Three different seal designs were tested in both calm and rough water. The bow seal designs consisted of a planing seal, a finger seal, and a bag and finger seal. The raw data from the tests yielded total forces acting on the bow and stern seals due to cushion pressure and aerodynamic and hydrodynamic influences. The model was instrumented in such a way as to allow the extraction of the total hydrodynamic seal drag (equivalent to the total seal drag being discussed here).

Knowing the total seal drag, the model operating conditions from the preceding tests, and the bow and stern seal attitudes, it was then possible to calculate the amount of total seal drag due to frictional effects. The difference between the total seal drag and the frictional seal drag is the seal-induced drag. These calculations were carried out for a planing type bow seal configuration for a variety of velocities and sea conditions. Figure 18 shows how the seal drag scaling factor K_1

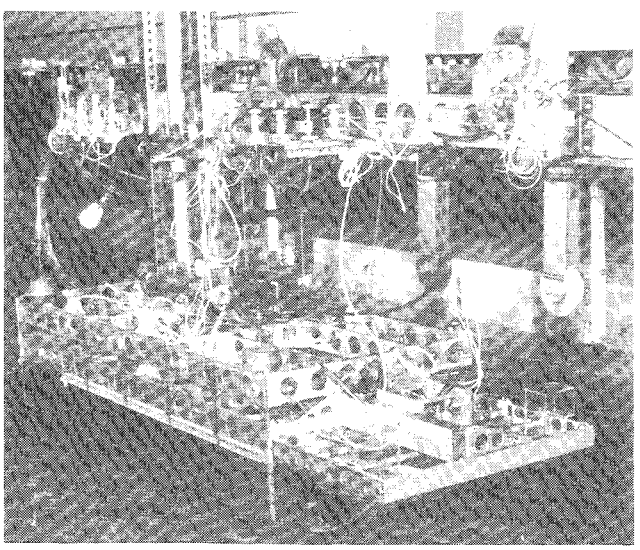

Fig. 16 Seal loads model.

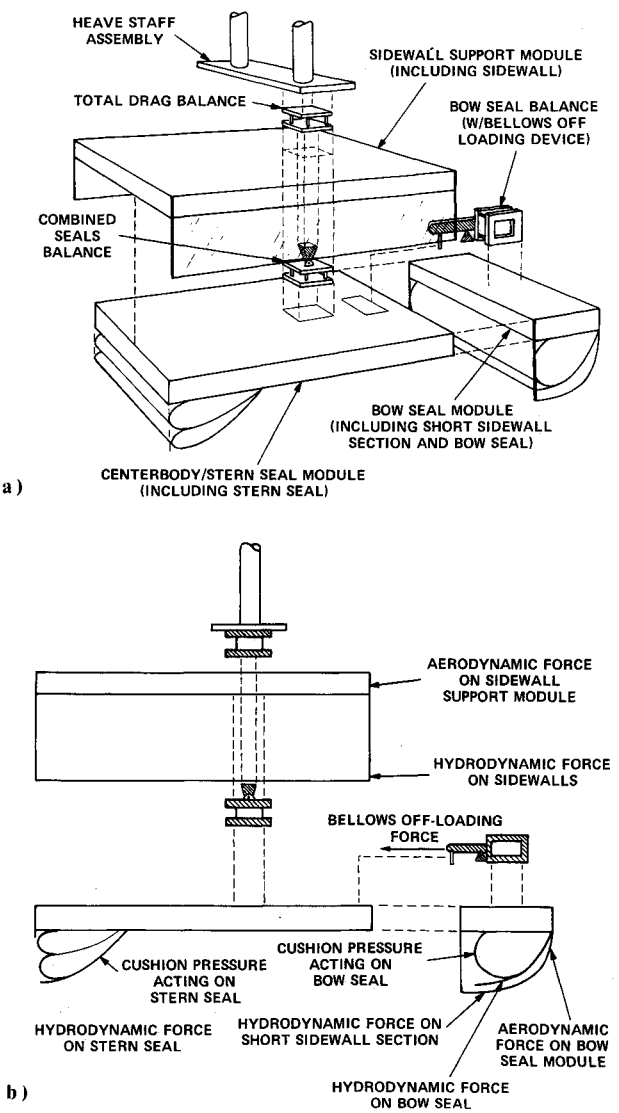

Fig. 17 Seal loads model components: a) schematic; b) forces.

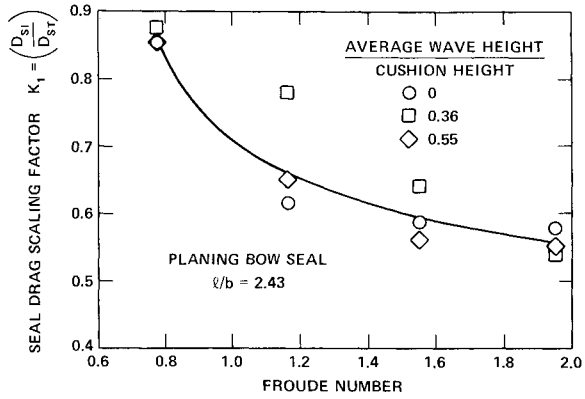

Fig. 18 Seal drag scaling factor variation with Froude number and wave height.

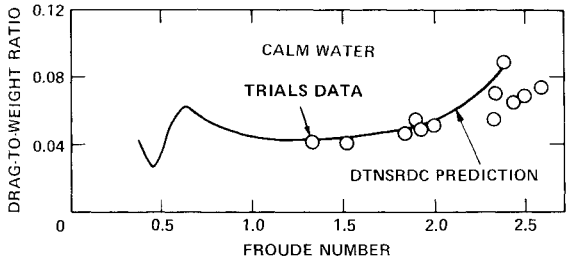

Fig. 19 Correlation of SES-100B data in a state 0 sea.

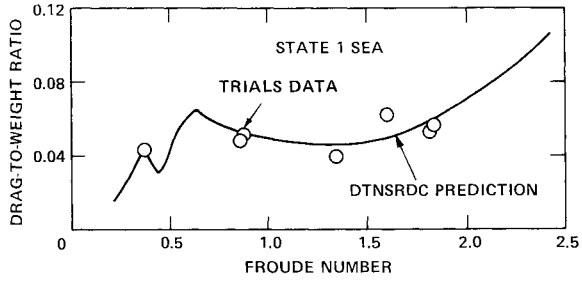

Fig. 20 Correlation of SES-100B data in a state 1 sea.

varies with ship Froude number for various sea conditions as determined from the seal experiments. The factor K_I is the ratio of the seal-induced drag D_{SI} to the seal total drag D_{ST}. The figure shows that there is a noticeable dependency of K_I on Froude number (or speed). However, the data generally collapse with respect to wave height variations. Although overall drag increases occur with sea state, the relative amounts of induced and frictional drag remain constant at particular velocities. Similar data exist for other seal types (finger, and bag and finger configurations), but are not presented here.

At present, expressions are being developed to accurately predict seal drag for the various seal designs previously described. When this is completed, residual drag (in the true sense of the word) will be very small and handled separately from the seal drag. However, at the present time, residual drag is scaled as follows:

$$\left(\frac{D_R}{W}\right)_P = \left(\frac{D_P}{W}\right)_M + \left[K_I + (1-K_I)\left(\frac{C_{f_P}}{C_{f_M}}\right)\right]\left(\frac{D_{ST}}{W}\right)_M$$

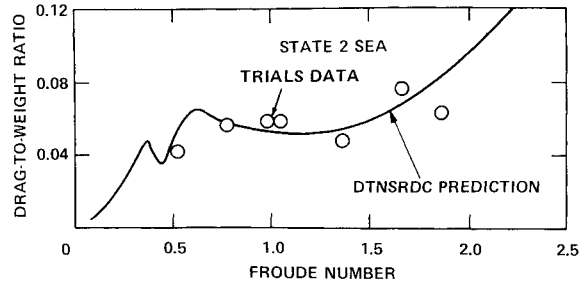

Fig. 21 Correlation of SES-100B data in a state 2 sea.

This expression separates the seal drag into its two components by virtue of the K_I term. Then, that part corresponding to frictional drag $(1-K_I)$ is scaled utilizing Reynolds scaling; that part corresponding to the induced drag K_I is Froude scaled as is the sidewall and appendage form and pressure drag.

Scaling Technique Correlation

The technique discussed in this paper has been used to compare scaled model data with full-scale trials data from the SES-100B. The SES-100B trials were conducted similar to model experiments, evaluating the effects of weight, longitudinal center-of-gravity location, airflow rate, and sea state. The model experiments in seas were run in the same scaled stationary wave spectrum measured during the trials program. The data are presented in Figs. 19-21 for state 0, 1, and 2 seas, respectively. The solid line is the scaled, faired model data while the data points are trials data. The data are presented in terms of drag-to-weight ratios because the trials data apply to varying weights due to fuel burnoff. These three figures show the adequacy of the scaling technique.

As further data become available, trials data from the SES-100A with modified seals and sidewalls will be compared to scaled model data to further verify the scaling technique. In addition, data from the XR-5 trials will be compared to scaled model data to verify the scaling routines relative to higher length-to-beam ratio surface effect ship designs.

References

[1] Ford, A. G., "Progress in Air Cushion Vehicles," David Taylor Model Basin Rept. 2280, Oct. 1966.

[2] Newman, J. N. and Poole, F. A., "The Wave Resistance of a Moving Pressure Distribution in a Canal," David Taylor Model Basin Rept. 1619, March 1962.

[3] Hogben, N., *Research on Hovercraft Over Calm Water*, Royal Institute of Naval Architects, Vol. 109, No. 3, July 1967, pp. 311-326.

[4] Hogben, N., "An Investigation of Hovercraft Wavemaking," *Journal of the Royal Aeronautical Society*, Vol. 70, No. 662, Feb. 1966, pp. 321-329.

[5] Williams, R. M., "Study of the Wavemaking of Captured Air Bubble Vehicles," Virginia Polytechnic Institute, Engineering Mechanics Dept. Rept., March 1968.

[6] Doctors, L. J., "The Wave Resistance of an Air-Cushion Vehicle," University of Michigan, Dec. 1970.

[7] Van Dyck, R. L., "Hump and Sub-Hump Performance Tests of a Surface Effect Ship, Phase I-Deep and Shallow Water Tests," Stevens Institute of Technology, Letter Rept. SIT-DL-72-1592, April 1972.

[8] Hoerner, S. F., *Fluid-Dynamic Drag*, 1965 ed. published by the author, Midland Park, N. J., 1958.

[9] Schlichting, H., *Boundary Layer Theory*, 6th ed., McGraw-Hill Book Co., Inc., New York, 1968.